A Generalized Accurate Modelling Method for Automotive Bulk Current Injection (BCI) Test Setups up to 1 GHz

Sergey Miropolsky, Alexander Sapadinsky, Stephan Frei
Technische Universität Dortmund, Germany
sergey.miropolsky@tu-dortmund.de

***Abstract* — Development of accurate system models of immunity test setups might be extremely time consuming or even impossible. Here a new generalized approach to develop accurate component-based models of different system-level EMC test setups is proposed on the example of a BCI test setup. An equivalent circuit modelling of the components in LF range is combined with measurement-based macromodelling in HF range. The developed models show high accuracy up to 1 GHz. The issues of floating PCB configurations and incorporation of low frequency behaviour could be solved. Both frequency and time-domain simulations are possible. Arbitrary system configurations can be assembled quickly using the proposed component models. Any kind of system simulation like parametric variation and worst-case analysis can be performed with high accuracy.**

Keywords — Automotive EMC, IC EMC, Virtual EMC Tests, Bulk Current Injection (BCI), Vectfit Macromodelling

I. INTRODUCTION

The EMC failures detected at the test-and-measurement stage may lead to expensive device redesigns and cause serious delays of a product launch. The success of a chip-level EMC test (e.g. Direct Power Injection, DPI, [1]) does not necessarily imply the success of a following system-level EMC tests (e.g. Bulk Current Injection, BCI, [2]). To evaluate the RF immunity at early design stages it is helpful to perform virtual EMC tests using accurate models. The variation of test setup parameters, e.g. cable harness length, is necessary for a worst-case analysis.

Models for system-level EMC setups have been developed by multiple groups e.g. [4-8]. In this work a generalised approach to develop an accurate component-based model of a system-level immunity test setup is described on the example of the bulk current injection (BCI) method. Equivalent circuit modelling in LF range is combined with measurement-based macromodelling in HF range. Any setup configurations can be assembled using the component models, thus parametric variation and worst-case analysis become possible.

According to [2] the BCI test is performed in the frequency range up to 400 MHz. The internal requirements often extend the range up to 1 GHz. The developed model must also support transient simulations involving RF and LF signals. Therefore the model must be valid from LF (DC) up to at least 1 GHz.

II. BULK CURRENT INJECTION (BCI) TEST SETUP

The bulk current injection for system-level applications (ISO 11452-4, [2]) is widely used for RF immunity testing of electronic components, especially in automotive industry. The sketch of such test setup is shown in fig. 1.

The equipment under test (EUT) consisting of a test PCB with one or more ICs to be tested is connected to the peripheral equipment with a cable harness of a specified length. The EUT is usually floating, i.e. it is not grounded locally, but only connected to the peripheral devices with a long cable harness. The PCB is coupled to ground due to stray fields. An artificial network (AN, LISN) is used to supply DC or LF signals or to measure the HF signal levels. Additional devices might be used to provide the LF functionality.

In the BCI test a common mode RF current of a specified amplitude or simply a specified forward power is injected into the cable harness using an injection clamp, and the EUT / DUT functionality is observed under this RF disturbance.

The setup modelling can be split into test-case dependent and independent parts. Many components involved in an RF immunity test, namely the LISN, the cable harness and the BCI injection clamp, should be modelled only once and can be re-used for further test cases. The supplementary equipment, PCB and DUT impedances are test-case dependent, therefore the models should be developed for each case individually. In some application cases the supplementary equipment is not used, the DC signals are supplied to the cable harness with the LISN and the DUT monitoring is performed with optically-decoupled probes. This configuration is considered in current work for simplicity purposes.

A cable harness of any type can be used in real BCI tests. A twisted pair cable harness will be considered in this work. A similar approach can be applied for any other cable type including homogenous cable bundles.

As it was proposed and confirmed by multiple authors [7,8,12], the test setup can be described as a complex multiple-port system. The goal of modelling is to reproduce the setup behaviour in a simulation environment.

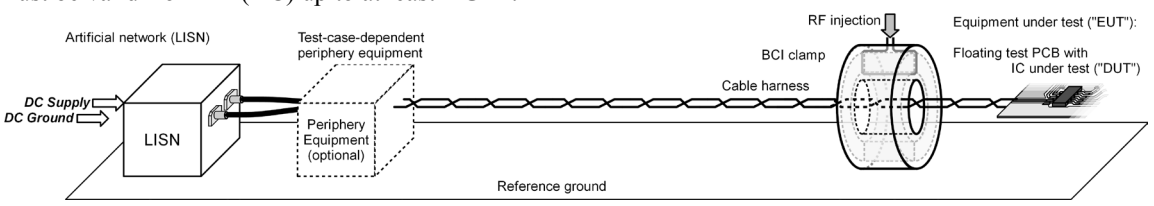

Fig. 1 System-level bulk current injection setup overview

III. Modelling Methods for Passive Components

A. Equivalent circuit setup modelling

For some components the equivalent circuit models can be easily found in LF range. The model extension with parasitic couplings and precise parameters fitting extends the model validity to higher frequencies. Due to necessary simplifications, these models are usually valid up to 100-200 MHz.

B. Measurement-based macromodelling

Passive structures can be modelled with a measurement-based macromodelling method. The device network parameters are measured with a network analyser (VNA), approximated with rational functions [9], converted to a state-space model, and implemented as a circuit [11]. The macromodels reproduce the passive electrical behaviour as it was captured at the original measured object. Commonly a high accuracy can be reached, whereby it depends on the quality of the measurement dataset, data approximation order, and circuit implementation.

This method shows high efficiency and accuracy, but has several drawbacks. The frequency range and dynamic impedance range covered by the model do not exceed those of the VNA (commonly from 300 kHz up to 1 GHz and from 10 mΩ up to 1 MΩ). The lower frequency limit is important, since many properties necessary for transient simulation can only be captured in LF range. The measurement-based data artefacts might be approximated within the original dataset. Another significant method limitation is the necessity of a 50 Ω measurement access to all involved nodes. This is especially critical for EMC setups with floating PCBs due to the missing common ground connection. Finally, the measurement-based macromodels can only reproduce the transfer function of an existing physical setup. For any parameter variation of e.g. cable harness length or injection clamp position, the entire modelling procedure must be repeated completely.

C. Proposed combined modelling procedure

The advantages of both methods can be used to develop the combined simulation models [11]. The component must be characterized with VNA measurement up to the highest involved frequency, e.g. 1 GHz. Precise deembedding might be used to exclude the influence of test fixtures or other irrelevant components. An equivalent circuit model must be created to be valid from DC up to at least the lowest frequency covered with the measurement data, e.g. 100 MHz. The circuit parameters should be optimized so that a smooth transition of simulation model to VNA measurement data is observed in the boundary frequency range for each S-, Y- and Z-parameter curve.

The scattering network parameter datasets of LF simulation (DC to e.g. 100 MHz) and the deembedded HF measurement (e.g. 100 MHz to 1 GHz) must be concatenated. The data smoothness at the edge frequency can be enforced by using a linear or low order polynomial transition from LF to HF data in some frequency window around the boundary frequency. A Vectfit approximation [9] can now be applied to this concatenated dataset [11] and a macromodel can be generated. The macromodels based on such combined datasets show correct results in the range from DC to 1 GHz and can be used in both frequency and time domain simulations.

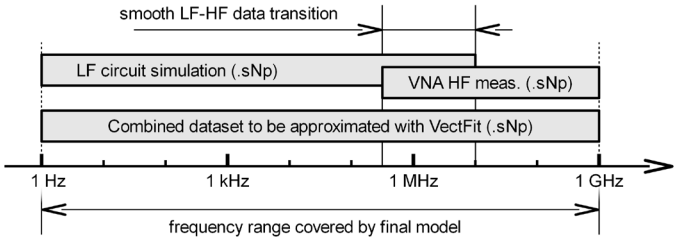

Fig. 2 S-parameter dataset concatenation for combined macromodelling

IV. BCI Component-Based Setup Modelling

The test setup is modelled with an electrical circuit (fig. 11) consisting of parameterised sub-circuits of cable harness, BCI coupling, LISN and floating PCB with DUT.

A. Cable harness: multiconductor TL model

The cable harness is one of the most important components of the test setup. In most existing models for BCI setups, e.g. [5-6], a quasi-TEM mode signal propagation along the cable harness is assumed. The cable harness is modelled with a multiconductor transmission line (MTL). Circuit simulators, e.g. Synopsys HSPICE, provide good support for MTL devices, so the model of this type is used for simulation. The MTL devices in HSPICE can be described with per-unit-length RLCG parameters. The frequency dependencies are either listed in tabular form, or approximated using R_0, L_0, G_0, C_0, the skin effect R_S and the dielectric loss G_D [17] matrices.

Multiple methods for measurement-based characterisation of MTLs are available, e.g. [14]. A significant issue of all types of measurement-based MTL analysis is to separate the self-properties of a homogenous MTL from the test fixtures (fig. 3). The cable properties close to the fixtures are also different from those of the homogenous cable over ground due to the stray couplings to the fixtures. A high parameter extraction accuracy for both homogenous cable harness and stray fields is critical for further deembedding procedures. Therefore a very high attention should be paid to this seemingly-simple step.

B. BCI coupling modelling

Multiple injection clamp models have been developed, e.g. [3-6]. Here the circuit model for the BCI clamp (FCC F140) was developed similar to [6]. The parameters were found by fitting the circuit model to measurement data. The coupling to the secondary and tertiary windings was considered to be concentrated at a single cable point and implemented with an ideal three-port transformer as shown in [4]. The clamped cable (7 cm) was initially included as an MTL with the same RLCG values as for the cable over ground.

A precise 5-port dataset of the BCI coupling to the cable was obtained by measurement of the setup shown in fig. 4 and a deembedding procedure. The test fixture RF ports were deembedded as lossless 60 ps port extensions. The cable with stray effects at the fixtures and the remaining cable harness were deembedded up to the side plane of the BCI clamp, so that the ports of the dataset were connected between the cable pins and the ground (ports 2-5 in fig. 4). The procedure was repeated for three cable lengths (15, 20 and 25 cm). The same dataset (up to numerical noise and smaller measurement artefacts) was obtained after deembedding. Thereby the deembedding method validity and accuracy were assured.

The smaller differences in the RLCG properties of the clamped cable to those of the main harness were extracted and implemented into the MTL model. The same setup was assembled and simulated in HSPICE and the S-parameters

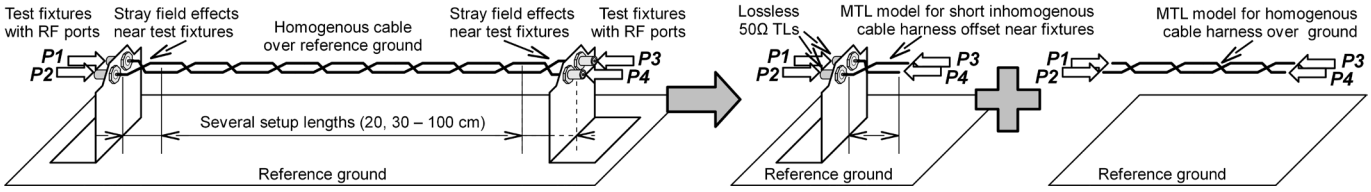

Fig. 3 Twisted cable harness characterization: measurement setup (left) and goal models for separate setup components (right)
The procedure of the parameter extraction method for homogenous cable harness and test fixture offsets will be shown in details in the coming publications.

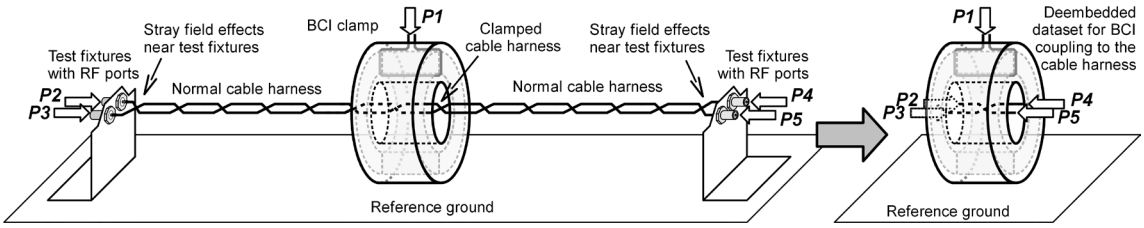

Fig. 4 BCI coupling to a twisted cable characterisation – measurement setup (left) and deembedded 5-port dataset (right)

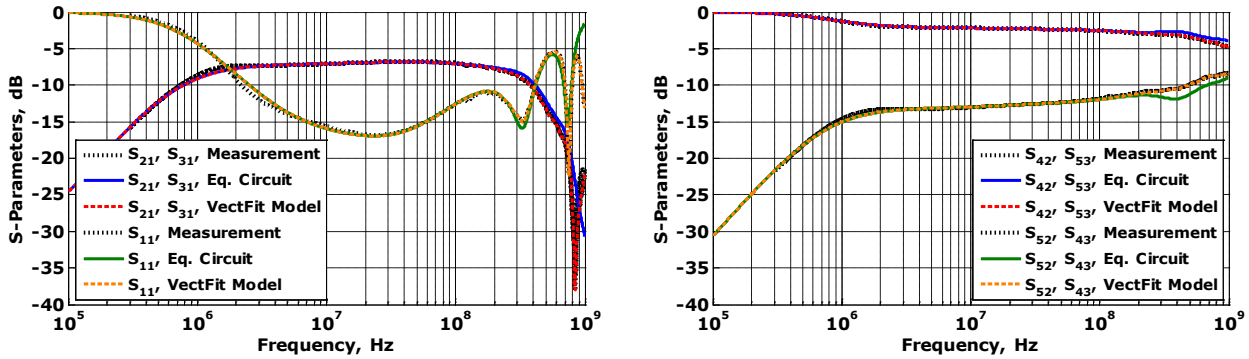

Fig. 5 BCI clamp model vs. deembedded dataset a) BCI port reflection and coupling to cable b) signal transfer through the cable within BCI clamp

were compared with measurements (fig. 5). A good correlation could be observed up to at least 400 MHz, while the internal BCI clamp resonance at 800 MHz was missing in the model.

To extend the model validity up to 1 GHz, the simulated dataset (1 Hz to 400 MHz) was concatenated with the deembedded measurement dataset (100 MHz to 1 GHz). A smooth linear transition was enforced in the range of 100 to 400 MHz. The concatenated dataset was approximated with vector fitting [9] to a macromodel. The S-parameters for the BCI coupling were simulated with the model and compared to the deembedded data (fig. 5). High model accuracy in the entire frequency range up to 1 GHz could be reached.

C. HF artificial network (AN / LISN)

A common LISN device specified in [2] must have an input impedance of 50 Ω at the cable harness port up to 108 MHz. The properties in higher frequency range are unspecified. It is possible to model an existing LISN device in the HF range using the same combined macromodelling approach. However, clean RF measurements are not possible without additional measures because of the specific non-RF connectors at available LISNs. Also by reproducing the HF issues of a LISN in a model, the known measurement problems are simply transferred into the virtual EMC tests.

A LISN with a 50 Ω input impedance and smooth transfer functions up to 1 GHz was designed (fig. 6). The SMD devices reproduce the LF behaviour. The 50 Ω PCB traces handle the signal transfer in HF range. All LISN ports are designed as RF connectors to allow device characterization with VNA. A circuit model for such device is easily developed up to 1 GHz.

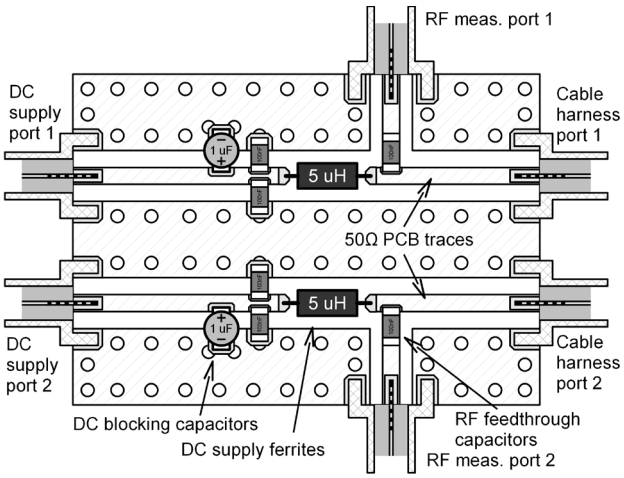

Fig. 6 HF artificial network (LISN) internal structure

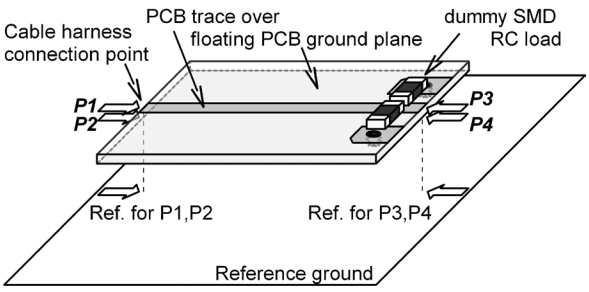

Fig. 7 Dummy EUT: floating test PCB with a single trace and dummy DUT (here: SMD RC load of 100 nF || 1 kΩ)

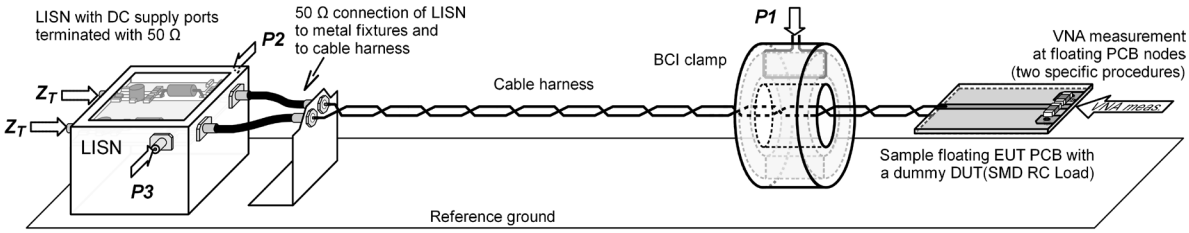

Fig. 8 Test setup for verification of developed models, BCI injection into cable harness with LISN and floating PCB with dummy RC load
Note, that signal transfer in the setup depends not on the setup only, but also on the measurement ports assignment.

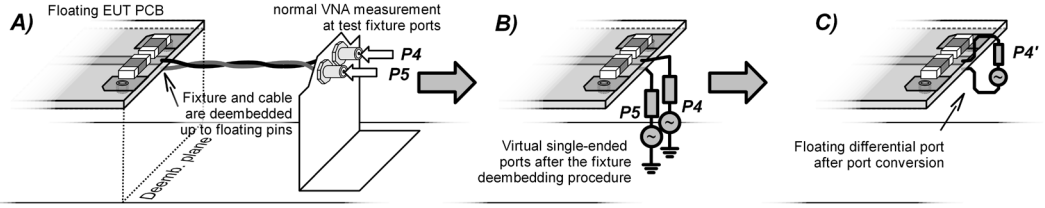

Fig. 9 Measurement of small-signal transfer function to the floating PCB nodes by deembedding the pre-characterized metal fixtures and short cable harness
A) Measurement structure with test fixtures B) Single-ended ports to reference ground after deembedding C) Floating differential port after port conversion

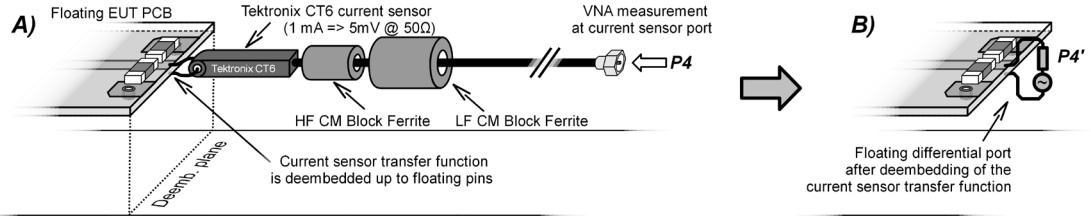

Fig. 10 Measurement of small-signal transfer function to the floating PCB nodes by deembedding the pre-characterized small-size current sensor
A) Measurement structure with current sensor B) Floating differential port after current sensor deembedding
The technical details and possible issues of the mentioned deembedding and port conversion procedures will be shown the coming publications.

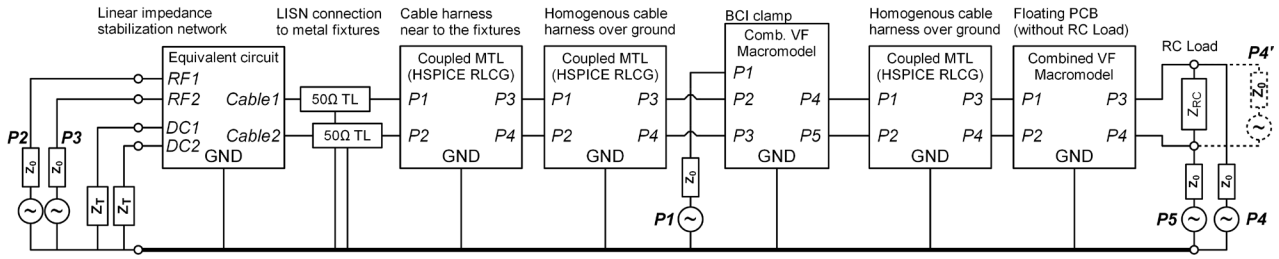

Fig. 11 Simulation model with two possible port assignments: a 5-port setup with single-ended ports P_4 and P_5 and a 4-port setup with a differential port P_4'

D. Floating test PCB modelling

One of the significant problems in modelling the system-level BCI setups is a floating PCB. According to the specification, the EUT is located in 50 mm height above the ground and is connected to the cable harness. Plastic EUT packages do not affect the couplings and therefore can be neglected for modelling. Hence the EUT can be reduced to a test PCB with an IC under test and, optionally, some SMD periphery necessary for LF functionality or RF protection.

The common-mode RF current injected is converted into a differential-mode signal due to the asymmetric impedances at the floating PCB. This CM-DM conversion was analysed in details in [13]. Starting with approx. 100 MHz a distributed conversion should be considered. In real test cases the 3D simulation of the PCB can be performed with an EM field solver. The virtual ports should be defined between the floating nodes, e.g. at the trace nodes, at the IC pins, and at the relevant points of the PCB ground plane. The S-parameter dataset can be simulated, approximated and used in the further simulation.

A simplified test PCB with a single signal trace over PCB ground is used in current work (fig. 7). The complex model of the CM-DM signal conversion at floating conductors can be simplified to an asymmetric MTL model with an approach similar to [13], where the PCB ground is considered to be just one more conductor over main reference ground.

The floating PCB structure without SMD components is measured in test fixtures in the same way as in section IV.B. The fixtures and the cable are precisely deembedded and a 4-port dataset of the floating PCB is obtained. The virtual ports are connected between the floating nodes and ground (fig. 7). The combined Vectfit macromodel is developed for the structure in the same way as discussed in section III-C.

E. DUT and dummy RC load modelling

To exactly reproduce a real RF immunity test, a physical transistor-level IC model has to be combined with a package model and must be attached to the ports of the floating PCB model. Since IC modelling for RF immunity testing is a separate complex topic which should not be covered within this work, a simple linear load of 1 kΩ || 100 nF is used here. The load is represented by two SMD components soldered between signal trace and PCB ground as shown in fig 7. The load impedance is measured with a VNA, modelled with a simple passive equivalent circuit, and connected to the corresponding pins of a floating PCB model.

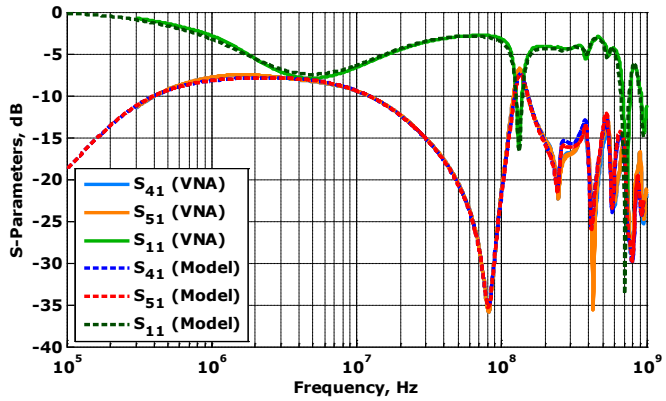

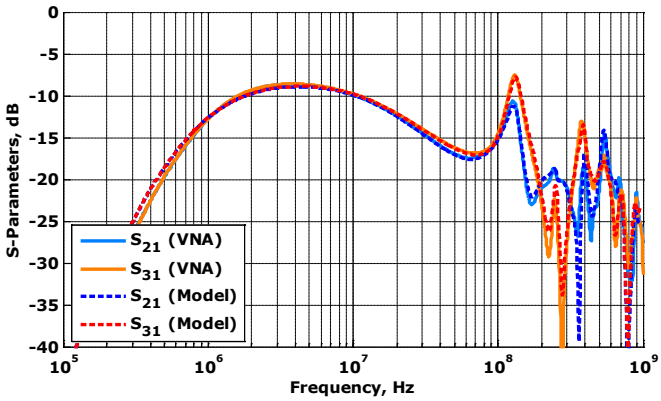

Fig. 12, 13 Signal coupling to LISN and PCB ports in the first configuration with single-ended ports to reference ground (P_4, P_5 in fig. 8, 9B)

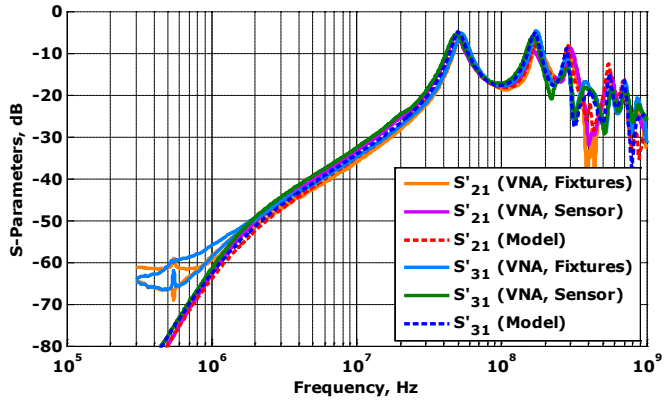

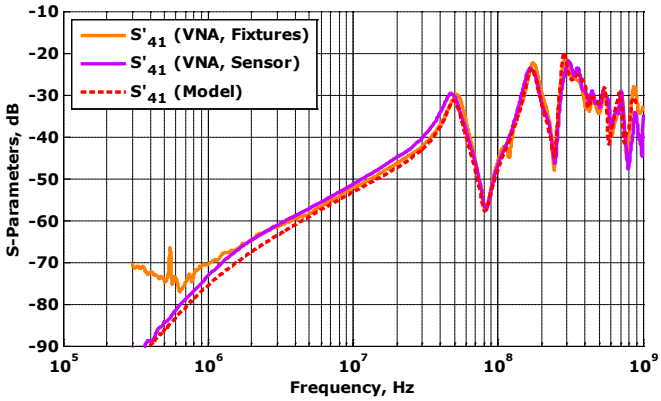

Fig. 14,15 Signal coupling to LISN and PCB ports in the second configuration with a floating differential port (P_4' in fig. 8, 9C, 10B) obtained by current sensor deembedding (fig. 10A-B) and by fixture deembedding and port conversion (fig. 9A-C)

V. MODEL VERIFICATION

The modelling approach is verified with measurements. The verification setup, consisting of 1m cable harness, LISN and dummy floating EUT with passive RC load, is assembled as shown in fig. 8. Two short 50 Ω cables are used to connect the LISN to the test fixture ports. The BCI clamp is located in 15 cm distance from the edge of the floating EUT PCB.

A significant issue to be handled during model verification is to access the floating PCB nodes. A physical connection of a VNA port is not possible due to obvious reasons. Two following solutions were used.

A. Deembedding cable harness up to floating PCB nodes

The floating pins can be accessed by precise deembedding. The metal fixtures (section IV.A) are connected to the PCB pins with a 5 cm piece of the cable harness. The measurement is performed up to fixture ports (fig. 9A). The fixtures and the cable are then deembedded as in section IV.B. The resulting single-ended 50 Ω ports are attached between the floating nodes and the ground (fig. 9B). By applying a port conversion procedure to two single-ended ports, the signal transfer to the *floating differential port* P4' can be obtained (fig. 9B,C).

B. Floating differential measurement using current sensor

In the second method the usage of the metal fixtures is avoided. A current sensor (Tektronix CT6) is used to transform the pin-to-pin current into the signal at the VNA port (P_4' in fig. 10A).The transfer function of the sensor is deembedded [15,16]. The resulting *floating differential port* is attached between the cable pins (P_4' in fig. 10B). The method presumes that the floating nodes are not disturbed by the sensor. Still some additional CM impedance to ground ("to infinity") is introduced into the system, and cannot be deembedded in this configuration. This CM impedance can still be characterized by measuring the current sensor in a known setup and can be appended to the simulation model for the comparison purposes.

The results for both methods are compared to each other to assure the methods validity, and to the simulation results.

C. Results and discussions

The simulation and measurement results for the test setup in the first configuration with two single-ended ports (P_4 and P_5 in fig. 8, 9B) are shown in fig. 12-13. A closed common mode (CM) current loop is present in the system due to two 50 Ω ports to the main reference ground at the floating PCB nodes (P_4, P_5 in fig. 9B). The BCI magnetic coupling induces significant CM current in the cable harness. Therefore a high signal level is observed at all setup ports already in LF range.

This configuration with virtual single-ended ports doesn't correspond to a typical BCI application with floating EUT, but can be efficiently used to validate the model. The simulated BCI coupling to the virtual ports between the floating pins and the ground (S_{41}, S_{51}) shows very good correlation to the measurement even in HF range. The same accuracy can be observed for the coupling to LISN ports (S_{21}, S_{31}). The signal transfer between other setup nodes (e.g. from floating PCB to LISN ports) also show sufficient accuracy. The rest curves are not shown here due to brevity purposes.

The results for the second setup configuration with floating port (P'_4 in fig. 9C and 10B) are shown in fig. 14-15. Here the common mode current loop in the system is open, and the

magnetic coupling induces a high CM voltage (but not the CM current) over the cable harness. Therefore a weak LF coupling is observed in LF range (S'_{21}, S'_{31}, S'_{41} in fig. 14-15). With rising frequency the capacitive coupling of the floating PCB to main reference ground increases, and the CM current rises. This leads to the increasing signal at LISN ports (S'_{21}, S'_{31}). The impedance asymmetry leads to the appearance of the differential signal at the cable harness in general and locally at the floating port (S'_{41}). Starting with 100 MHz the signal transfer is determined by cable resonances.

Both measurement methods show the same results (up to two insignificant deviations) in the entire frequency range. The measurement with fixtures shows an artefact in LF range (below 1 MHz). This is caused by the applied port conversion, which is rather sensitive to the VNA measurement noise, especially for the analysis of weak differential signals.

The current sensor measurement in its turn shows a smaller offset in signal levels in LF range from 5 to 50 MHz. This signal offset is caused by the current sensor CM impedance (approx. 0.5 – 0.75 pF with some HF losses). By characterising this impedance with a separate measurement and deembedding procedure, modelling it with a simple equivalent circuit and attaching it to the single-ended ports before the port conversion an even better model correlation to the measurements can be reached for verification purposes.

A very good fitting can be observed for both measurement methods and simulation models. Even for the signal transfer to the floating differential port, which is normally very complex to both measure and model in such configurations, a good correlation of model to measurement data is observed. This confirms the accuracy of both measurement methods and the simulation model.

VI. Model application

The developed test setup model can be used in virtual EMC test during IC design. Here a floating PCB model has to be created for each test case e.g. with EM field solver. The IC models (either transistor-level or behavioural) wrapped in package models have to be attached to the floating PCB nodes, and the circuit simulations of any kind can be performed. The test setup model can also be efficiently used for substitution methods mentioned in [7,8,12].

The main advantage of a component-based EMC test setup model is the possibility to simulate any test configuration, including different cable harness lengths and clamp positions, passive protection at PCB level, complex cable networks, etc., purely virtually, i.e. without running a real EMC test. A worst-case analysis can be performed. The EMC failures can be detected and necessary built-in IC solutions or an external PCB-level EMC protection can be developed in advance.

Conclusions

A generalized method to develop an accurate component-based model of a system-level BCI test setup is proposed. The components are characterized with VNA measurements and precise deembedding. An equivalent circuit modelling in LF range is combined with measurement-based macromodelling for HF range. Such models are valid in the up to 1 GHz for both frequency and time domain simulations.

The setup model is verified with measurements. Two independent measurement procedures are used to capture the signal transfer to a dummy DUT (RC load) at the floating PCB. Both methods confirm the accuracy of the simulated results.

The models can be used for advanced EMC simulations involving complex transistor-level or behavioural DUT models. The EMC failures can be detected and necessary built-in IC solutions or an external PCB-level EMC protection can be developed in advance.

Acknowledgement

The reported R+D work was carried out within the CATRENE project CA310 EM4EM (Electromagnetic Reliability and Electronic Systems for Electro Mobility). This particular research is supported by the BMBF (Bundesministerium fuer Bildung und Forschung) of the Federal Republic of Germany under grant 16 M3092 I. The responsibility for this publication is held by the authors only.

References

[1] IEC 62132-4: Integrated circuits – Measurement of electromagnetic immunity, part 4: Direct Power injection (DPI) method.

[2] ISO 11452-4: Road vehicles – Component test methods for electrical disturbances from narrowband radiated electromagnetic energy, part 4: Bulk current injection (BCI)

[3] M. F. Sultan, “Modeling of a bulk current injection setup for susceptibility threshold measurements,” IEEE Int. Symp. on EMC Proceedings, San Diego, CA, 1986, pp. 188-195.

[4] F. Grassi, F. Marliani, S. A. Pignari, “Circuit Modeling of Injection Probes for Bulk Current Injection,” IEEE Tran., EMC 49, no. 3, Aug. 2007, pp. 563-576

[5] F. Lafon, Y. Belakhouy, and F. De Daran, “Injection probe modeling for bulk current injection test on multiconductor transmission lines,” IEEE Symp. on Embedded EMC Proceedings, Rouen, France, 2007.

[6] Miropolsky, S., Frei, S., and Frensch, J.: Modeling of Bulk Current Injection Setups for Virtual Automotive IC Tests, EMC Europe, 2011, Wroclaw, Poland, 2011.

[7] Durier, A., Pues, H., Vande Ginste, D., Chernobryvko, M., Gazda,C., and Rogier, H.: Novel Modeling Strategy for a BCI setup applied in an Automotive Application, EMC Compo 2011, Dubrovnik, Croatia, 2011.

[8] Oguri, Y., Ichikawa, K.: Simulation Method for Automotive Electronic Equipment Immunity Testing, EMC Europe 2012, Rome, Italy, 2012.

[9] Gustavsen, B., Semlyen, A.: Rational Approximation of Frequency Domain Responses by Vector Fitting, IEEE Tran. On Power Delivery, 14, 1052–1061, 1999.

[10] The Vector Fitting Website, http://www.sintef.no/projectweb/vectfit

[11] Miropolsky, S., Frei, S., Optimierung der Makromodellierung von Übertragungsstrecken mit Vector-Fitting-Methoden durch Anpassung der Eingangsdaten, EMV Düsseldorf, 2014 (accepted for publication)

[12] Miropolsky, S. and Frei, S.: Comparability of RF Immunity, Test Methods for IC Design Purposes, EMC Compo 2011, Dubrovnik, Croatia, Nov. 2011.

[13] Crovetti, P. S., Fiori, F.: Distributed Conversion of Common-Mode Into Differential-Mode Interference, IEEE Tran. on Microwave Theory, Vol. 59, No. 8, Aug. 2011.

[14] Degerstrom, M.J., B.K. Gilbert, and E.S. Daniel. Accurate resistance, inductance, capacitance, and conductance from uniform transmission line measurements, IEEE-EPEP, 18th Conf., Oct. 2008, pp. 77–80.

[15] zur Nieden, F, Frei, S., Pommerenke, D., "A combined impedance measurement method for ESD generator modeling, EMC Europe 2011 York , vol., no., pp.476-481, Sept. 2011

[16] zur Nieden, F., Scheier, S., Frei, S., "Circuit models for ESD-generator-cable field coupling configurations based on measurement data, EMC Europe 2012, 17-21 Sept. 2012

[17] Synopsys HSPICE User Guide on Signal Integrity Modelling and Analysis, version F-2011.09, September 2011